17th Brazilian Congress of Thermal Sciences and Engineering
November 25th-28th, 2018, Águas de Lindóia, SP, Brazil

ENCIT-2018-0177
THERMAL ANALYSIS AT BLUNT BODY OF THE GENERIC SCRAMJET FLYING AT 30 KM ALTITUDE WITH MACH NUMBER 6.8

Paulo Gilberto de Paula Toro
Emanuel Vieira Mendes
Jonatha Wallace da Silva Araújo
George Santos Marinho
Universidade Federal do Rio Grande do Norte/UFRN - Centro de Tecnologia. Av. Senador Salgado Filho, 3000 - Campus Universitário, Lagoa Nova CEP 59.078-970 – Natal/RN - Brasil
toro@ct.ufrn.br; emanuel-mendes@hotmail.com; jonatha_wallace@hotmail.com; gmarinho@ct.ufrn.br

Gilvan Luiz Borba
Universidade Federal do Rio Grande do Norte/UFRN - Centro de Ciencias Exatas e da Terra. Av. Senador Salgado Filho, 3000 - Campus Universitário, Lagoa Nova, CEP 59.078-970 - Natal, RN - Brasil
gilvan@geofisica.ufrn.br

Felipe Jean da Costa
Instituto Tecnológico de Aeronáutica/ITA - Praça Marechal Eduardo Gomes, nº 50 Vila das Acácias CEP. 12.228-900 São José dos Campos, SP – Brasil
felipejean15@hotmail.com

Israel da Silveira Rêgo
Instituto de Estudos Avançados/IEAv - Trevo Coronel Aviador José Alberto Albano do Amarante, nº1 Putim CEP. 12.228-001 São José dos Campos, SP - Brasil
israel.rego@ieav.ct.br

Abstract. *A generic hypersonic airbreathing propulsion based on supersonic combustion ramjet (scramjet) technology has been designed, at the Universidade Federal do Rio Grande do Norte (UFRN), using analytical theoretical analysis (engineering approach). Aerospace vehicles flying at hypersonic speeds (corresponding to Mach number higher than 5) undergo a process of temperature increase at the structural wall of the vehicle and surrounding. A full-scale generic scramjet model configuration is based on the technological demonstrator scramjet 14-X S, in development at the Instituto de Estudos Avançados (IEAv). A two-dimensional hydrogen powered generic scramjet has been designed to demonstrate, in atmospheric flight, a supersonic combustion, of atmospheric air (in supersonic speed) with hydrogen, on an acceleration mission to 2050 m/s (Mach number 6.8) at 30 km geometric altitude. Knowledge of the phenomenon of aerodynamic heating is of paramount importance to estimate the surface temperature, and to the material specification to be used for its manufacture, its thermal protection that keeping the wall temperature and in the external and internal surface temperatures of vehicle at acceptable levels. Fay and Riddell and Lees methodologies are used to evaluate the aerodynamic heating at the stagnation point and blunted-nose, respectively, considering under calorically perfect (γ=1.4) gas. External surface temperature at the stagnation point and blunted-nose, considering Inconel 718 material and thickness of the structural materials of the scramjet are presented.*

Keywords: *scramjet, supersonic combustion ramjet, hypersonic airbreathing propulsion, thermal analysis*

1. INTRODUCTION

In March 2012, the coordination of the scramjet 14-X project proposed the design of the 14-X S, with two compression ramps (Fig. 1) to demonstrate the scramjet technology at 30km altitude with Mach number 7 (using the Brazilian solid rocket engines S31 and S30), which the external configuration is based on 14-X waverider and scramjet engine experimental data as well as on the one-dimensional theoretical analysis.

In 2013, Martos et al. (2017) developed experimental investigation of the half of the 14-X S model, at T3 Hypersonic Shock Tunnel, which was scaled based on the 14-X S design to fly at Mach number 7 and 30 km of altitude (Fig. 1). Martos et al. (2017) observed, in some experimental runs, the separation of the boundary-layer due to boundary layer and shock wave interaction between first and second ramps of the inlet, but not the reattachment of it.

The original 14-X S consists a two-dimensional configuration (Fig. 1), with a constant cross-section (Fig. 2), which shows only the half of the constant cross-section. The scramjet surface consists of a frontal surface with a leading-edge

angle of 5.5º, compression ramp angle of 14.5º (related to the angle of the leading edge), the internal expansion chamber combustion angle of 4.27º and external expansion angle of 10.73º (related to the angle of internal expansion).

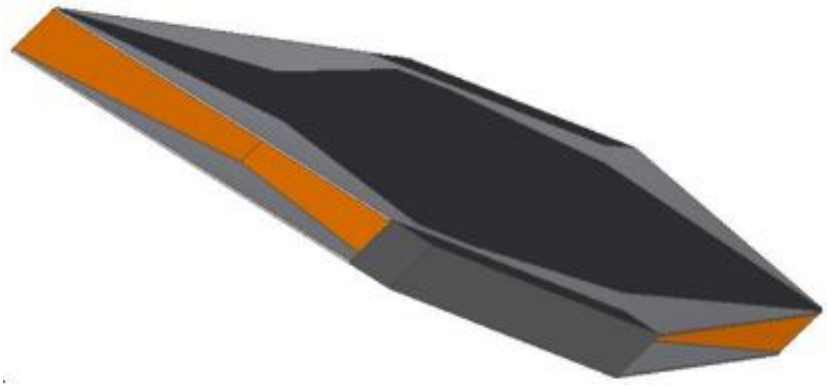

Figure 1. Scramjet 14-X S configuration with two compression ramps.

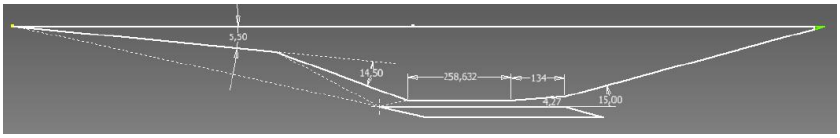

Figure 2. Cross-section of the 14-X S (with two compression ramps) flying at 30km altitude at Mach number 7.

According to Heiser and Pratt (1994) for Mach 7 the maximum angle between these two ramps should be around 12º to minimize the boundary layer separation. The separation of the boundary layer is critical for a hypersonic inlet because it changes shock wave angle, pressure recovery, and heat transfer while may lead to chocked flow even resulting in unstart of the engine. The half of the 14-X S model has a turning angle of 14.5º between its compression ramps, such that for some experimental conditions were possible to observe the separation of the boundary layer but not the reattachment of it.

In 2014, the Coordination of the Brazilian scramjet 14-X project, at the Instituto de Estudos Avançados (IEAv), decided to design a new version of the scramjet 14-X S (Fig. 2), with three compression ramps, instead two compression ramps (Fig. 1), to demonstrate the scramjet technology to fly in the Earth's atmosphere, at 30km altitude and velocity corresponding the Mach number 6.8. Additionally, a blunt region (with radius of 1mm) at the leading-edge of the scramjet 14-X S was added due to manufacture purpose and to prevent high aerodynamic heating at the tip of the 14-X S with sharp leading-edge.

In order to assure the reattachment of the boundary layer and to minimize the boundary layer and shock wave interaction effects a new version of the 14-X S with three ramps was designed to fly at a Mach number 6.8 through Earth's Atmosphere at 30 km geometric altitude. The scramjet inlet consists of three compression ramps with the turning angles of 5.5° (to be consistent with the leading-edge of the scramjet 14-X S with two ramps) following by two ramps with the turning angles of 7° and 8.5° (Fig. 3).

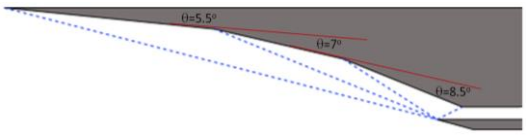

Figure 3. Cross section of the generic scramjet inlet.

In the contemporary space research, the challenges posed by aerospace activities are the full knowledge of the environment and of phenomena founds in the hypersonic flight of the aerospace vehicles. In particular the atmosphere offers resistance to movement of the vehicle, converting a large portion of kinetic energy in thermal energy. Thermal energy generated results in large heat flux causing a substantial temperature increase in the atmosphere surrounding the outer surface of the vehicle the order of hundreds of degrees Celsius. The knowledge of aerodynamic heating phenomenon is important to design a system of thermal protection that keep the wall (internal and external) surface temperatures of space vehicle at acceptable levels.

Hypersonic flight introduces extreme thermal loads on the leading-edges of the vehicle, which generates high temperature around the vehicle surfaces. Consequently, high temperature materials and high temperature coatings

should be employed, that have particularly structural, aerodynamic and thermal protection function (Harsha et al., 2005). The extreme thermal loads on the leading-edges of the vehicle have a significant magnitude in terms of heat flux. The heat flux increases inversely to the square root of the nose radius (Fay and Riddell, 1956).

2. METHODOLOGY

2.1 Scramjet characteristics

Firstly, a nomenclature was defined to be used in the analytical theoretical analysis. Following Heiser and Pratt (1994) the 14-X S may be divided in three (Fig. 4) main components: external and internal compression section (inlet), combustion chamber (combustor) and internal and external expansion section (outlet). Also, the hypersonic vehicle with airframe-integrated scramjet engine may be divided by several stations (Fig.4).

Stations 0 and 1 are the leading edges of the scramjet and of the cowl, respectively. Stations 3 and 4 are the entrance and exit of the combustion chamber. Stations 9 and 10 are the trailing edges of the cowl and the scramjet, respectively.

The external compression section is governed by incident shock wave, while the internal is governed by reflected shock wave. The internal and external expansion section is governed by expansion wave, Prandtl-Meyer Theory, and area ratio. The constant area section of the combustion chamber is called as isolator and is used to uniformize the flow from the compression section. Fuel is injected right after the isolator used to expand the gases from burning the fuel and the oxygen. In general, one-dimensional flow with heat addition, Rayleigh flow, is used to simulate the burning the fuel and the oxygen.

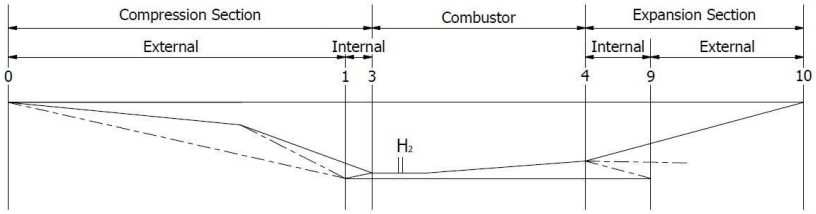

Figure 4. Scramjet engine stations and reference terminology, adapted from Heiser and Pratt (1994).

Note that the incident shock waves (Fig. 4), from the external compression section, should incident on the leading-edge of the cowl (shock on-lip) and the reflected shock wave, of the internal compression section, should incident on the entrance of the combustion chamber (shock on-corner). Therefore, the air capture area should be maximum and the length of the scramjet compression section should be minimum.

2.2 Surface energy balance

The exchange of energy (in transit) between any solid structural material and the environment atmosphere is due to a temperature difference (Fig. 5) and involves the three basic forms of heat transfer: conduction, convection, and radiation.

Conduction heat transfer, which is governed by Fourier heat conduction law (Eq. 1), occurs across the medium (solid or a stationary fluid), and it is proportional to the temperature gradient. Convection heat transfer is governed by Newton's law of cooling (Eq. 2) and occurs between a surface and a moving fluid when both are in different temperatures. Radiation heat transfer occurs from all surfaces of finite temperature which emit energy in form of electromagnetic waves and it is the Stefan-Boltzmann law (Eq. 3).

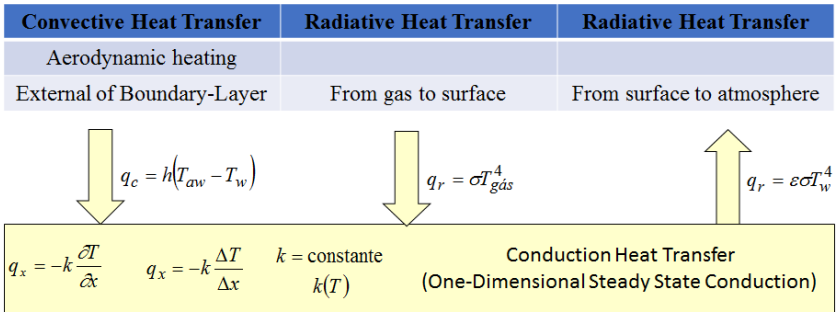

Figure 5. The energy balance for conservation of energy at the scramjet wall surface.

$$q_x = -k\frac{\partial T}{\partial x} \tag{1}$$

$$q_c = h\left(T_{aw} - T_w\right) \tag{2}$$

$$q'' = \varepsilon\sigma\left(T_2^4 - T_1^4\right) \tag{3}$$

2.3 Aerodynamic heating governing equations

Fay and Riddell (1958) presents the theory of heat transfer in dissociated air applying to a blunt body stagnation point given by

$$q = \frac{0.763}{(\mathrm{Pr})^{0.6}}(\rho_s\mu_s)^{0.4}(\rho_w\mu_w)^{0.1}(H_s - h_w)\left[1 + \left(Le^{0.52} - 1\right)\frac{h_d}{H_s}\right]\left[\left(\frac{du_e}{dx}\right)_s\right]^{0.5} \tag{4}$$

$$\left(\frac{du_e}{dx}\right)_s = \frac{1}{R}\sqrt{\frac{2(p_s - p_\infty)}{\rho_s}} \tag{5}$$

where the subscript *s* indicates the properties at the stagnation point, ∞ indicates the properties of the free stream and *w* indicates the properties of the wall surface.

Lees (1956) presents the laminar heat transfer over blunt-nosed hypersonic flight speeds, related to the stagnation point heat transfer (Eq. 4), given by

$$\frac{\dot{q}_w}{\left(\dot{q}_w\right)_0} = \frac{2\cdot\theta\cdot\mathrm{sen}\,\theta\left\{\left[1 - \left(\frac{1}{\gamma\cdot M_\infty^2}\right)\right]\cos^2\theta + \frac{1}{\gamma\cdot M_\infty^2}\right\}}{[D(\theta)]^{\frac{1}{2}}} \tag{6}$$

$$D(\theta) = \left(1 - \frac{1}{\gamma\cdot M_\infty^2}\right)\left(\theta^2 - \frac{\theta\cdot sen4\theta}{2} + \frac{1-\cos 4\theta}{8}\right) + \frac{4}{\gamma\cdot M_\infty^2}\left(\theta^2 - \theta\cdot sen2\theta + \frac{1-\cos 2\theta}{2}\right) \tag{7}$$

2.4 Thermodynamic flow property governing equations

2.4.1. Normal shock wave relations

Considering no boundary-layer effects (inviscid flow) and for calorically perfect gas ($p = \rho RT$, $\gamma = \text{constant}$) the normal shock wave relationships (Fig. 6)can be easily obtained as closed form of the thermodynamic property (static pressure, static density, static temperature, …) ratios and Mach number across the normal shock given by:

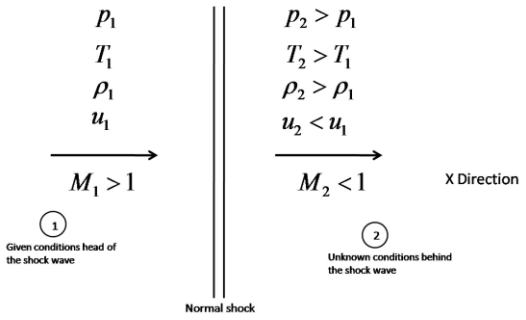

Figure 6. Normal shock wave geometry.

$$\frac{p_{out}}{p_{in}} = 1 + \frac{2\gamma}{(\gamma+1)}\left[\left(M_{in}\,sen\beta\right)^2 - 1\right] \tag{7}$$

$$\frac{\rho_{out}}{\rho_{in}} = \frac{(\gamma+1)\left(M_{in}\ sen\beta\right)^2}{\left[(\gamma-1)\left(M_{in}\ sen\beta\right)^2+2\right]} \tag{8}$$

$$\frac{T_{out}}{T_{in}} = \frac{p_{out}}{p_{in}}\ \frac{\rho_{in}}{\rho_{out}} = 1+\frac{2\gamma}{(\gamma+1)}\left[\left(M_{in}\ sen\beta\right)^2-1\right]\frac{\left[(\gamma-1)\left(M_{in}\ sen\beta\right)^2+2\right]}{(\gamma+1)\left(M_{in}\ sen\beta\right)^2} \tag{9}$$

$$M_{out} = \frac{\sqrt{\dfrac{\left(M_{in}\ sen\beta\right)^2+\dfrac{2}{(\gamma-1)}}{\dfrac{2\gamma}{(\gamma-1)}\left(M_{in}\ sen\beta\right)^2-1}}}{sen\left(\beta-\theta_s\right)} \tag{10}$$

where: ρ, p, u, and h are density, pressure, velocity and enthalpy of the gas across the normal shock wave, respectively.

Note, the flow across the normal shock wave promote an increase of pressure, density, temperature, and a decrease of Mach number for lower than 1.

2.4.2. Planar oblique shock wave relations

Considering no boundary-layer effects (non-viscous flow) and for calorically perfect gas ($p=\rho RT$, $\gamma=\text{constant}$) the shock wave angle β (Fig. 7) is a function of the incoming local supersonic/hypersonic flow Mach number M_{in}, the gas from the atmosphere γ (air in the Earth's planet, $\gamma=1.4$) and the deflection angle θ_s , and it may be obtained iteratively with the relationship given by (Anderson, 1990):

$$tg\theta_s = 2\left(\text{cotg}\,\beta\right)\left[\frac{\left(M_{in}\ sen\beta\right)^2-1}{M_{in}^2\left(\gamma+\cos 2\beta\right)+2}\right] \tag{11}$$

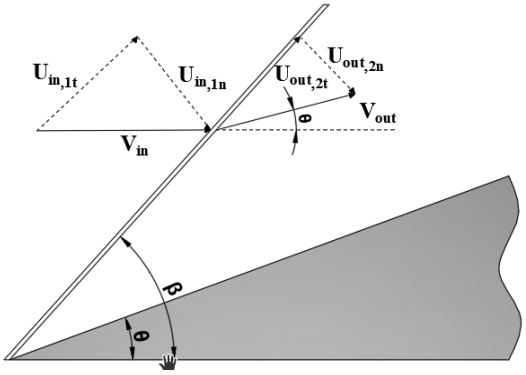

Figure 7. Leading edge incident plane oblique shock wave geometry.

Additionally, the oblique shock relationships can be easily obtained as closed form of the thermodynamic property (static pressure, static density, static temperature, …) ratios and Mach number across the oblique shock given by:

$$\frac{p_{out}}{p_{in}} = 1+\frac{2\gamma}{(\gamma+1)}\left[\left(M_{in}\ sen\beta\right)^2-1\right] \tag{12}$$

$$\frac{\rho_{out}}{\rho_{in}} = \frac{(\gamma+1)\left(M_{in}\ sen\beta\right)^2}{\left[(\gamma-1)\left(M_{in}\ sen\beta\right)^2+2\right]} \tag{13}$$

$$\frac{T_{out}}{T_{in}} = \frac{p_{out}}{p_{in}} \quad \frac{\rho_{in}}{\rho_{out}} = 1 + \frac{2\gamma}{(\gamma+1)}\left[\left(M_{in}\ sen\beta\right)^2 - 1\right] \frac{\left[(\gamma-1)\left(M_{in}\ sen\beta\right)^2 + 2\right]}{(\gamma+1)\left(M_{in}\ sen\beta\right)^2} \tag{14}$$

$$M_{out} = \frac{\sqrt{\dfrac{\left(M_{in}\ sen\beta\right)^2 + \dfrac{2}{(\gamma-1)}}{\dfrac{2\gamma}{(\gamma-1)}\left(M_{in}\ sen\beta\right)^2 - 1}}}{sen\left(\beta - \theta_s\right)} \tag{15}$$

Note, the flow across the oblique shock wave promote an increase of pressure, density, temperature, and a decrease of Mach number, however the flow remains supersonic/hypersonic and parallel to the flat surface of the external and internal compression section (Fig. 7) of the hypersonic vehicle with airframe-integrated scramjet engine lower surface.

2.5 Thermal Analysis

Heat transfer may occur in one or more of its three basic forms: conduction, convection, and radiation. The Fourier heat conduction law states that the heat flow is proportional to the temperature gradient. Convection heat is the energy transport affected by the motion of a fluid. Newton's law of cooling governs the convection heat transfer between two dissimilar media. For convection the heat flow is proportional to the difference of the temperatures of two media. Convection heat transfer coefficient or film conductance is the proportionality constant. The radiant or electromagnetic energy emitted by a medium is unique to the temperature of the medium; this is defined as thermal radiation. The Stefan-Boltzmann law describes the radiant exchange between surfaces or region, and the radiant energy transmitted is proportional to the difference of fourth power of the temperatures of the surfaces, this proportional parameter is called Stefan-Boltzmann constant. The Laplace equation is the three-dimensional flow governing equation of heat into a solid in steady-state. It can be used to describe the thermal response of the structure. For 3-D Conduction Heat Transfer is given by

$$\frac{\partial}{\partial x}\left(k\frac{\partial t}{\partial x}\right) + \frac{\partial}{\partial y}\left(k\frac{\partial t}{\partial y}\right) + \frac{\partial}{\partial z}\left(k\frac{\partial t}{\partial z}\right) - \rho cp\frac{\partial T}{\partial t} = 0 \tag{16}$$

where, ρ is the density, c_p is specific heat at constant pressure of the solid, k is thermal conductivity of the solid and T is the conduction heat flux in the *x, y* and *z* directions, respectively.

The temperature distribution may affect appreciably the material properties such as modulus of elasticity and the coefficient of thermal expansion (CTE). For the finite element analysis is needed to accommodate the temperature dependent properties that are based on the element average temperature and assumed constant within an element. To consider temperature dependent properties is needed a material database from a thermo-structural characterization, and thus, for the materials used for the scramjet 14-X (Costa et al., 2016). The access for this database has several difficulties, fact for which it was chosen to use the constant material properties according to supplier datasheets (Tab. 1).

Table 1. Thermal properties of isotropic materials.

	CTE [μm/ m-°C]	Specific Heat Capacity [J/g-°C]	Thermal Conductivity [W/m-K]	Melting Point [°C]	Emissivity
Inconel 718	13.0	0.435	11.4	1260 - 1336	0.58
Tungsten	4.40	0.134	117	3370	0.23
Titanium Alloy	8.90	0.528	17.0	1650 - 1670	0.63
Copper Alloy	24.8	0.385	400	1083.2 - 1083.6	0.66

The boundary conditions used for steady-state analysis are the aerodynamic heating from the Fay and Riddell (1958) and Lees (1956) theories, which provide the heat flux over the blunt body vehicle surface.

3. RESULTS AND COMMENTARIES

First is necessary to define the thermodynamic atmospheric air properties, which the generic scramjet will perform atmospheric flight, at 30 km geometric altitude (Tab. 2) and speed corresponding to Mach number 6.8 (Tab. 3).

Table 2. Thermodynamic atmospheric properties at 30 km altitude (U.S. Standard Atmosphere, 1976).

Altitude	Temperature	Pressure	Density	Mean free path	Sound speed	Dynamic viscosity
km	K	Pa	kg/m^3	m	m/s	N s /m^2
30	226.5	1197	0.01841	0.000004413	301.7	0.000014753

Table 3. Dimensionless quantities for Mach number 7 and 30 km.

Altitude	Knudsen number	Mach number	Velocity	Reynolds number
km	L=1 (m)		m/s	L=1 (m)
30	0.000004413	6.8	2051.6	2.56 10^6

Observe that the Knudsen number is very low, 4.413 10^{-6} ($Kn \leq 0.01$), so the mass, momentum and energy conservation laws, based on the Navier-stokes, should be applied for continuum flow (dense Earth's atmospheric air). Also, the flow over the scramjet is more like a turbulent flow with Reynolds number of 2.56 10^6.

The thermodynamic properties and airflow Mach number at the stagnation point, of the generic scramjet flying at 30 km altitude with Mach number 6.8 (2050 m/s), are estimated by the normal shock relations following the isentropic flow relations, considering no effects of boundary layer and the airflow behaves as calorically perfect gas (Fig. 8), therefore the velocity at stagnation point over the external surface of the generic scramjet must be zero. Also, the thermodynamic properties and airflow Mach number at the first ramps of the compression section are presented.

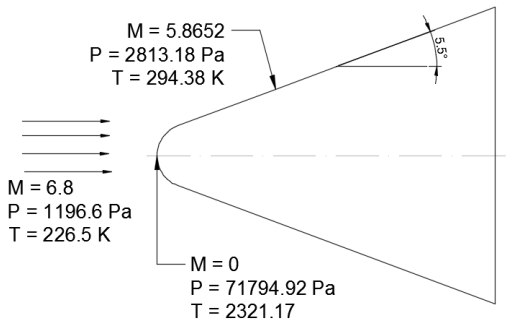

Figure 8. Thermodynamic properties at stagnation region of the blunt body of the generic scramjet inlet.

The thermal analysis is performed in a blunt body region of the generic scramjet (Fig. 9). Fay and Riddell (1958) and Lees (1956) theories were applied to the stagnation point and the cylinder section of the blunt body geometry (Fig. 9). The dimensionless laminar heat flux over scramjet blunt-nosed related with the stagnation point heat transfer is function of the geometric position along the blunt section (Fig. 9).

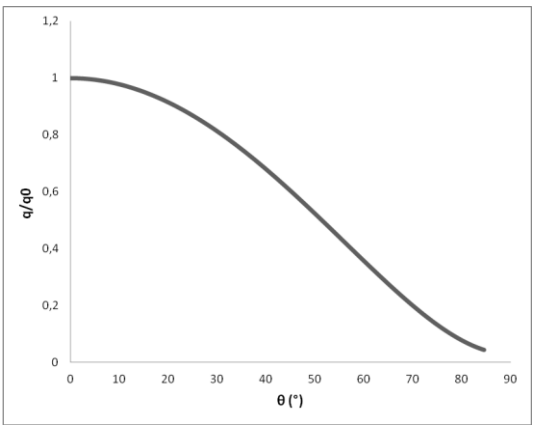

Figure 9. Aerodynamic heating (heat flux) along the blunt region.

The aerodynamic heating at the stagnation point of the scramjet blunt leading-edge estimate by Fay and Riddell (1958) is about $q_w^{\text{stagnation point}} = 4{,}428{,}700\,[\text{W/m}^2]$, considering the thermodynamic properties right after the normal shock wave following the isentropic flow. The aerodynamic heating estimated by Lees's theory present a senoidal behavior as one may have expected. The aerodynamic heating at the intersection of the cylinder section and the first ramp deflection of 5.5º is $q_w^{\text{intersection cylinder-ramp}} = 197{,}478.99\ [\text{W/m}^2]$.

The thermal analysis of the blunted region of the generic scramjet (Fig. 10) has been studied based on the external configuration and pressure distribution (Fig. 8) at Mach number 6.8 at 30km altitude. As show in Fig. 11, it was added some fins to better thermal response on the rear of the leading-edge part.

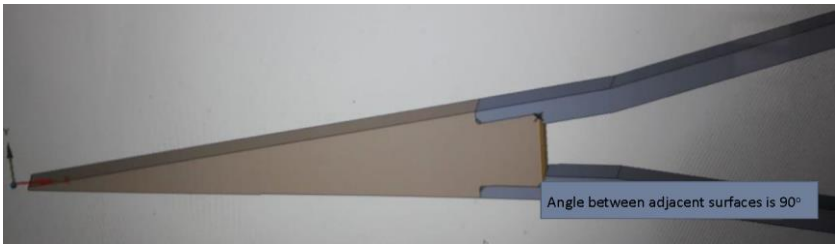

Figure 10. Generic scramjet configuration at the blunted region.

Considering the estimated aerodynamic heating, from stagnation point ($q_w^{\text{stagnation point}} = 4{,}428{,}700\,[\text{W/m}^2]$) to plane surface of the ramps at 5.5º ($q_w^{\text{intersection cylinder-ramp}} = 197{,}478.99\ [\text{W/m}^2]$) and using the Inconel 718 as the thermal structural material, the external surface temperatures at stagnation blunt region (Fig. 11) of the generic scramjet is higher (about 1586,6 K) than the material melting point (1336 K) of the Inconel 718 (Tab. 1). Besides that, the minimum temperature on the rear of the part is around 886,65 K.

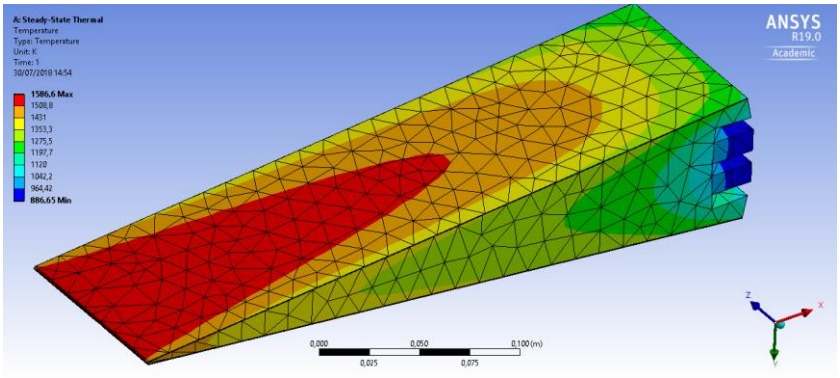

Figure 11. Temperature field over scramjet configuration at the blunted region using only Inconel 718.

Considering Copper Alloy, according with the properties presented in Tab. 1, the maximum temperature (1459,1 K) is higher than the material melting point (1083,6 K), as shown in Fig. 12. For this case, the minimum temperature is 1241,7 K, invalidating the usage of this material.

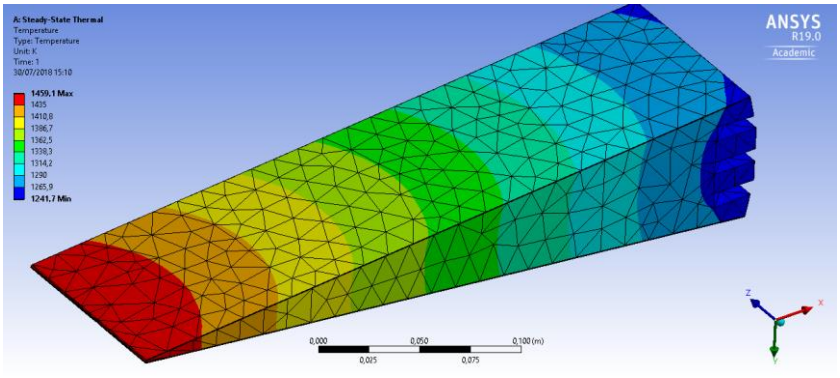

Figure 12. Temperature field over scramjet configuration at the blunted region using only Copper Alloy.

Considering now a Titanium Alloy, one can note the maximum temperature 1545,8 K and the minimum temperature was 964,9 K. It has a good thermal response, in the sense of to no overcome the melting point of the material (1670 K).

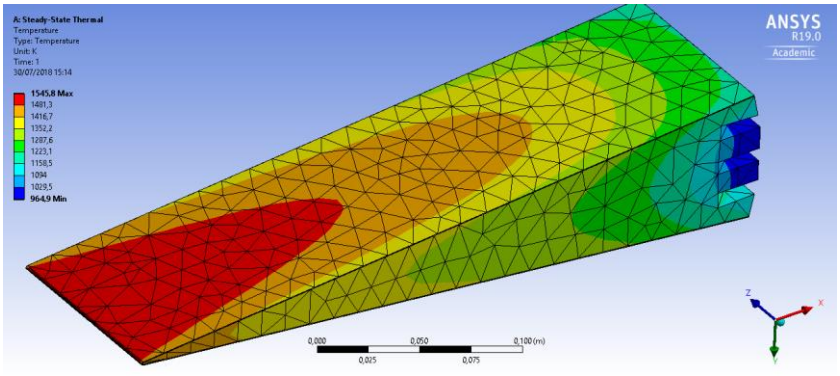

Figure 13. Temperature field over scramjet configuration at the blunted region using only Titanium Alloy.

Another case was studied, considering Tungsten and Inconel 718 materials, and dividing the part in two parts, which the thermal response is shown in Fig. 14. In this case the maximum temperature is 1398,4 K and the minimum temperature is 860,68 K. Note that in this case the maximum temperature (1338,4 K) on the Inconel 718 part is higher than the material melting point (1336 K).

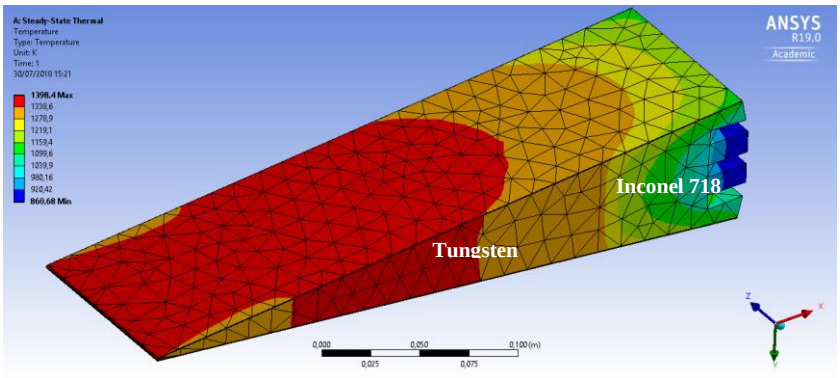

Figure 14. Temperature field over scramjet configuration at the blunted region using Tungsten and Inconel 718.

Applying 0,5 mm Thermal Barrier Coating (TBC) based on Alumina, at Titanium and Inconel 718 substrate, as thermal protection material the external temperature decreases at Inconel 718 part. The maximum temperature is kept at 1398,6 K and the minimum temperature decreases to 857,71 K. this case represents the better option of the material layout to face the thermal loads.

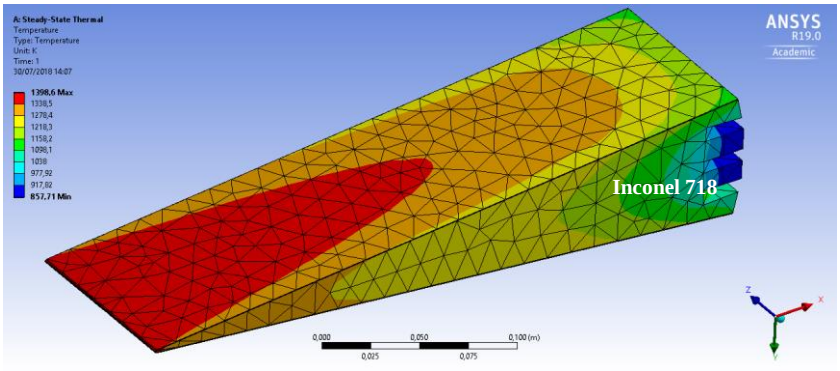

Figure 15. Temperature field over the external surface material of the blunt region using Titanium and Inconel 718, both with Alumina TBC.

4. CONCLUSION AND OUTLOOK FOR FUTURE PROJECTS

The primary objective of this work is to present the temperature distribution along of the thickness of the structural material of the blunt region scramjet configuration.

A full-scale generic scramjet model configuration is based on the technological demonstrator scramjet 14-X S, in development at the Instituto de Estudos Avançados (IEAv). A two-dimensional hydrogen powered generic scramjet has been designed to demonstrate, in atmospheric flight, a supersonic combustion, of atmospheric air (in supersonic speed) with hydrogen, on an acceleration mission to 2050 m/s (Mach number 6.8) at 30 km geometric altitude.

Based on the thermodynamic properties of the blunt body scramjet, aerodynamic heating data and structural material thermal properties the thermal analysis (heat flux and temperature) over blunted region are presented, considering for the structural materials.

Inconel 718 cannot hold lower temperature than the melting point when it is used as structural material and at the same time thermal protection material.

Also, it is studied the use of coating material (Copper Alloy) over the Inconel 718, which produces a maximum temperature itself higher than its melting temperature.

When Titanium Alloy is used as structural and thermal material it provides the maximum temperature 1545,8 K, which is lower than the melting temperature.

Considering Tungsten and Inconel 718 as structural and thermal materials, the maximum temperature was 1398,4, which is higher than the melting temperature of the Inconel 718.

The better solution is applying 0,5 mm Thermal Barrier Coating (TBC) based on Alumina, at Titanium and Inconel 718 substrate, as thermal protection material, so the external temperature decreases at Inconel 718 part. The maximum temperature is kept at 1398,6 K and the minimum temperature decreases to 857,71 K, which is lower than the melting temperature of the Inconel 718.

Further studies must develop including change structural material using, for example, Carbon-Carbon composite and heat pipe structures.

5. ACKNOWLEDGEMENTS

The first five authors would like to thanks to Universidade Federal do Rio Grande do Norte (UFRN) the support given to complete this scientific work. The first author (as Visiting Professor) would like to express appreciation to UFRN the possibility to apply the knowledge in aerothermodynamics and hypersonics in the research area in hypersonic airbreathing propulsion based on supersonic combustion ramjet (scramjet) technology. This work has been partially sponsored by Instituto Tecnológico de Aeronáutica and the sixth author would like to extend his appreciation to support this project. Finally, a portion of this effort was supported by Instituto de Estudos Avançados (IEAv) and by the Propulsão Hipersônica 14-X (PropHiper) Project and the last author would like express his appreciation.

6. REFERENCES

Anderson, J. D., Modern Compressible Flow, The Historical Perspective. McGraw-Hill, Inc., ed. 2nd, 1990.

Costa, F. J.; rêgo, I. S.; Minucci, M. A. S.; Toro, P. G. P. “Thermal Analysis of the Brazilian 14-X Hypersonic Aerospace Vehicle at Mach number 7”. In: CONEM 2016 - IX Congresso Nacional de Engenharia Mecânica, 21 a 25 de agosto de 2016, Fortaleza - Ceará

Heiser, W. H.; Pratt, D. T. *Hypersonic Airbreathing Propulsion*. Washington, D.C, American Institute of Aeronautics and Astronautics, 1994.

Martos, J. F. A. Aerothermodynamic design, manufacturing and testing of a 3-d prototyped scramjet. Thesis of Doctor in Science - Space Science and Technology, Space Propulsion and Hypersonics – Instituto Tecnológico de Aeronáutica, 2017.

Toro, P. G. P.; Carneiro, R.; Araújo, J. W. S, Marinho, G. S.; Borba, G. L.; Rego, I. S.; Martos, J. F. A., “Design and Analysis of a generic scramjet air inlet”. 17th Brazilian Congress of Thermal Sciences and Engineering (ENCIT 2018). November 25th-28th, 2018, Águas de Lindóia, SP, Brazil.

U.S. Standard Atmosphere. NASA TM-X 74335. National Oceanic and Atmospheric Administration, National Aeronautics and Space Administration and United States Air Force. 1976.

7. RESPONSIBILITY NOTICE

The authors are the only responsible for the printed material included in this scientific article.

The authors declare that there is no conflict of interest regarding the publication of this scientific article.